Partially gapped Fermi surfaces in $La_3Co_4Sn_{13}$ revealed by nuclear magnetic resonance

H. F. Liu,[1] C. N. Kuo,[1] C. S. Lue,[1,*] K.-Z. Syu,[2] and Y. K. Kuo[2,†]

[1]*Department of Physics, National Cheng Kung University, Tainan 70101, Taiwan*

[2]*Department of Physics, National Dong Hwa University, Hualien 97401, Taiwan*

(Received 14 June 2013; revised manuscript received 31 July 2013; published 9 September 2013)

We report a study of a single-crystal $La_3Co_4Sn_{13}$ by means of the specific heat and ^{59}Co nuclear magnetic resonance (NMR) spectroscopy. A first-order phase transition with a marked peak at $T^* \simeq 152$ K has been discerned by the specific heat measurement. The observed transition has been connected to a structural change from a simple cubic to a body-centered-cubic superstructure with crystallographic cell doubling, accompanied by the Fermi surface reconstruction. Indeed, NMR observations clearly indicate a significant change in the local electronic characteristics across this phase transition. The spin-lattice-relaxation rate measurement further provides an estimate of Co 3*d* Fermi-level density of states $N_d(E_F)$, revealing a visible reduction in $N_d(E_F)$ in the low-temperature phase. This finding essentially associated with the partially gapped Fermi surfaces would be appropriate for the isostructural analog of Sr_3Ir_4 Sn_{13}, which has been claimed to possess charge-density-wave (CDW) behavior with a three-dimensional crystallographic structure.

DOI: 10.1103/PhysRevB.88.115113 PACS number(s): 71.20.−b, 71.45.Lr, 76.60.−k

I. INTRODUCTION

Ternary stannides with the chemical formula $R_3T_4Sn_{13}$ (R = Ca, Sr, rare-earth element; T = Co, Rh, Ir) continue to attract attention in the field of solid state physics due to the existence of rich electronic and magnetic phenomena. Heavy fermions, mixed-valence behavior, complicated magnetism, as well as superconductivity have been found in this class of materials.[1–16] Within the superconducting catalog, $Ca_3Ir_4Sn_{13}$ and $Sr_3Ir_4Sn_{13}$ are prominent members with peculiar phase transition features in their normal states.[9,12–16] Anomalies in both electrical resistivity and magnetic susceptibility have been observed at $T^* \simeq 35$ K in $Ca_3Ir_4Sn_{13}$ and $T^* \simeq 147$ K in $Sr_3Ir_4Sn_{13}$. Single-crystal x-ray diffraction (XRD) analysis for Sr_3 Ir_4Sn_{13}below and above T^* confirms the presence of a structural change, with a lattice parameter twice than that of the high-temperature phase driven by the lattice distortion.[14] Such a lattice distortion was accompanied by the Fermi surface reconstruction which has been associated with the charge-density-wave (CDW) instability, responsible for the observed broad peak in the resistivity and a sudden drop in the susceptibility near T^*. The CDW scenario has also been adopted to the isoelectronic and isostructural $Ca_3Ir_4Sn_{13}$ compound.[15,16] By alloying these two systems, it allows one to study the competitive interplay between the CDW instability and superconductivity as the replacement of Sr with a smaller Ca atom would effectively produce chemical pressure in $Sr_3Ir_4Sn_{13}$. Indeed, a systematic suppression in T^* together with an enhancement in the superconducting transition temperature T_c has been found in the $(Ca_xSr_{1-x})_3Ir_4Sn_{13}$ alloys with increasing the Ca concentration.[14] Such an observation is in reminiscence of the behavior in $Lu_5Ir_4Si_{10}$, which has been confirmed to be a CDW superconductor in spite of its three-dimensional (3D) crystal structure.[17]

The titled compound of $La_3Co_4Sn_{13}$ crystallizes in a cubic $Yb_3Rh_4Sn_{13}$-type structure (space group $Pm\bar{3}n$) at room temperature, isostructural to $Sr_3Ir_4Sn_{13}$. There are two nonequivalent crystallographic tin atoms, termed as Sn1 and Sn2, within this crystal structure. Sn1, La, Co, and Sn2 atoms occupy the 2*a*, 6*d*, 8*e*, and 24*k* sites (in Wyckoff notations), respectively. The crystal structure of $La_3Co_4Sn_{13}$ is illustrated in Fig. 1. The bonding length of Co-Sn2 is the shortest among the nearest-neighbor atomic distances in $La_3Co_4Sn_{13}$, leading to the formation of the $Co(Sn2)_6$ trigonal prisms, which are corner sharing with a titled three-dimensional arrangement. Within the $Co(Sn2)_6$ trigonal prism environments, strong *p-d* hybridizationbetween Sn2 5*p* and Co 3*d* states occurs at around the Fermi level (E_F), as revealed from the band structure calculation.[18] According to the spin-polarized calculation, no significant spin splitting in 3*d* electronic bands takes place under the *p-d* hybridization.[18] It thus leads to a nonmagnetic character in $La_3Co_4Sn_{13}$, implying a low-spin state in Co atoms.

$La_3Co_4Sn_{13}$ has been found to be a superconductor with a low T_c of about 2.7 K.[5,6,19] Since the electrical resistivity and magnetic susceptibility exhibit no anomalous signatures above T_c, it is natural to classify $La_3Co_4Sn_{13}$ as an ordinary metal in its normal state.[5,6] Nevertheless, in the single-crystal XRD data of $La_3Co_4Sn_{13}$ below 150 K, Aguero *et al.* noted weak superstructural reflections indicating a structural change from a simple cubic to a body centered cubic superstructure with nearly doubling of the cell parameter.[20] Such a phenomenon bears a striking resemblance to that found in $Sr_3Ir_4Sn_{13}$.[14] In this regard, a raised question is whether an examination of the change of the electronic features in $La_3Co_4Sn_{13}$ will yield results similar to those in $Sr_3Ir_4Sn_{13}$, essential to elucidate the intriguing phase transition observed in the $R_3T_4Sn_{13}$ prototype.

In this paper, we report the specific heat (C_P) and ^{59}Co nuclear magnetic resonance (NMR) measurements on a single crystal $La_3Co_4Sn_{13}$ to shed light on the characteristics of the phase transition. It is known that the result of the specific heat could provide convincing classification of the nature of the phase transition.[21] Moreover, NMR is a local probe yielding information about Fermi surface features, giving reliable estimate for the change of the electronic density of states (DOS) at E_F.[22] In $La_3Co_4Sn_{13}$, a first-order phase transition at $T^* \simeq 152$ K was discerned in C_P. The NMR characteristics further provided microscopic evidence for the

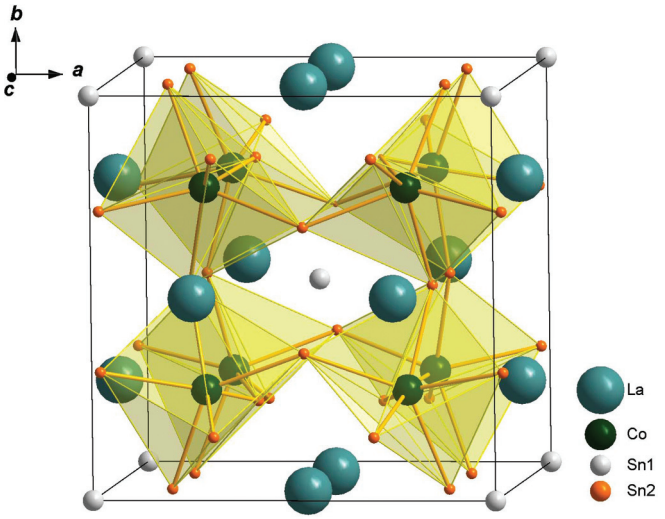

FIG. 1. (Color online) The crystal structure of $La_3Co_4Sn_{13}$ at room temperature. The structure highlights the arrangement of the corner sharing $Co(Sn2)_6$ trigonal prisms.

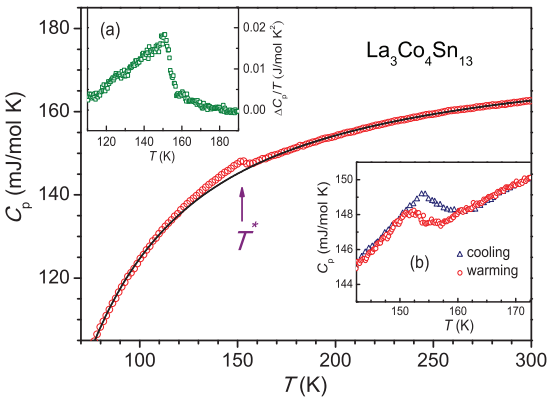

FIG. 3. (Color online) Temperature variation of the specific heat C_P for $La_3Co_4Sn_{13}$. The solid curve represents the background estimated by fitting the lattice specific heat through the experimental data far from the transition region. Inset (a) shows a $\Delta C_p/T$ vs T plot in the vicinity of T^*. Inset (b) displays thermal hysteresis behavior for the phase transition.

decrease in the Co 3d electronic states below T^*. Remarkably, the analysis of the NMR spin-lattice relaxation rates below and above T^* revealed a quantitative reduction of about 7.7% in the Co 3d DOS at E_F, associated with a nesting of Fermi surfaces along a particular wave-vector direction.

II. EXPERIMENTAL DETAILS

Single crystals of $La_3Co_4Sn_{13}$ were grown by the Sn self-flux method. High-purity elements were mixed in the molar ratio of La : Co : Sn = 1 : 1 : 20 and sealed in an evacuated quartz tube. The tube was heated up to 1273 K, dwelled for 5 h, and then cooled to 773 K over 25 h. The excessive Sn flux was etched in diluted hydrochloric acid. The obtained crystals have dimensions of $1\times 1\times 1$ mm^3. A room-temperature XRD measurement taken with Cu K_α radiation on the powdered single-crystal specimen was identified within the expected cubic $Yb_3Rh_4Sn_{13}$-type phase (space group $Pm\bar{3}n$),[23] as displayed in Fig. 2.

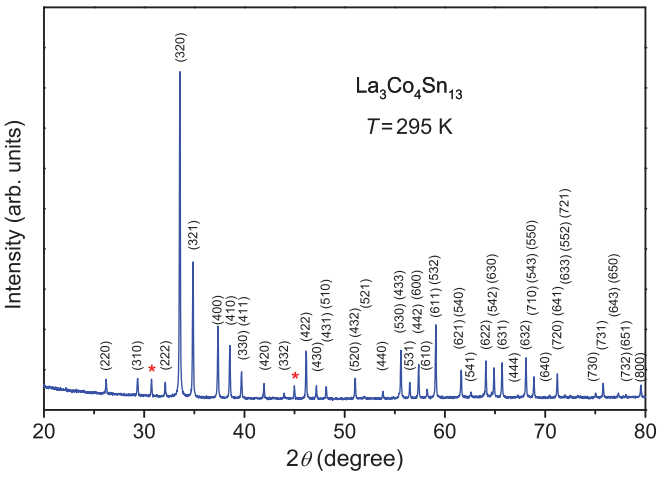

FIG. 2. (Color online) X-ray diffraction pattern for the powdered single-crystal $La_3Co_4Sn_{13}$. Reflections are indexed with respect to the $Yb_3Rh_4Sn_{13}$-type structure (space group $Pm\bar{3}n$). Impurity peaks marked by asterisks arise from excessive Sn.

Specific heat measurement was performed with a high-resolution ac calorimeter, using chopped light as a heat source. The ac technique is known to be one of the powerful tools for the study of small changes in the heat capacity of materials at their phase transitions, with a great precision and only a small size of sample needed. Further details about the experimental technique can be found elsewhere.[24] The observed temperature variation of the specific heat for $La_3Co_4Sn_{13}$ is shown in Fig. 3. A distinctive peak in C_p demonstrates the appearance of a phase transition at $T^* \simeq 152$ K. The observation confirms that the phase transition is an intrinsic property of $La_3Co_4Sn_{13}$ rather than the consequence arising from impurity phases. To evaluate the change of the entropy during the phase transition, we first determined the excess specific heat ΔC_p by subtracting a smooth background, estimated by fitting the lattice specific heat through the experimental data far from the transition region. The temperature dependence of $\Delta C_p/T$ around the phase transition is given in the inset of Fig. 3. A small entropy change $\Delta S \simeq 0.062R$ (where R is the ideal gas constant) was obtained by integrating $\Delta C_p/T$ through the entire transition region. We also found $\Delta C_p/C_p \simeq 1.6\%$ at T^*, indicting that the phase transition occurs at T^* in $La_3Co_4Sn_{13}$ is rather weak. The feature of thermal hysteresis in the vicinity of T^* is illustrated in the inset of Fig. 3, suggesting the first-order nature of this transition. This phase transition can be accounted for by the cell-doubling crystallographic structural transformation noted by Aguero and co-workers.[20]

In this investigation, NMR measurements were carried out using a Varian 300 spectrometer, with a constant field of 7.082 T. A home-built probe was employed for both room-temperature and low-temperature experiments. To avoid the skin depth problem of the rf transmission power, we crushed the single crystal and put the specimen in a plastic vial that showed no observable ^{59}Co NMR signal.[25] The Knight

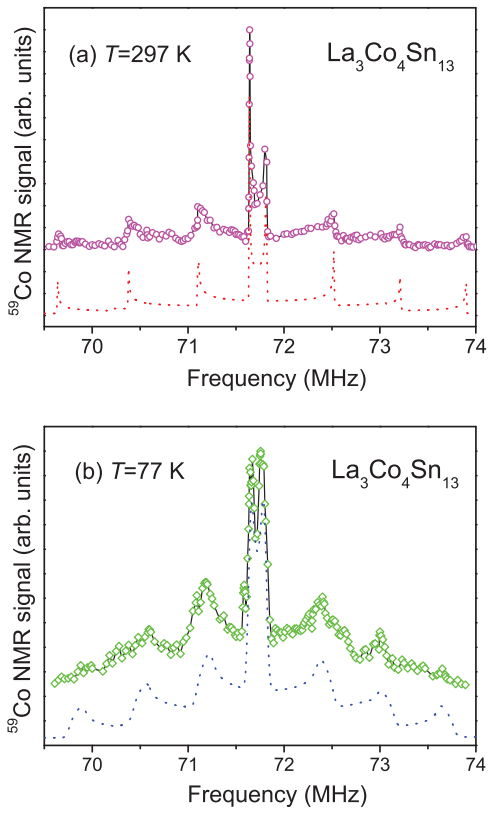

FIG. 4. (Color online) Fully resolved ^{59}Co NMR spectra for $La_3Co_4Sn_{13}$ measured at (a) 297 and (b) 77 K, respectively. Each simulated result plotted as a dashed curve is offset for clarity.

shift here was referred to the ^{59}Co resonance frequency of one molar aqueous $K_3Co(CN)_6$.

Since the ^{59}Co NMR resonance is quadrupolar broadened, each wide-line spectrum was mapped out by integrating spin echo signal of various excitations. In Figs. 4(a) and 4(b), we presented two fully resolved powder patterns of $La_3Co_4Sn_{13}$ taken at 297 and 77 K, respectively. Due to electric quadrupole coupling, the ^{59}Co NMR spectrum ($I = \frac{7}{2}$) consists of seven transition lines. It is clear that the sharpness of each transition line edge slightly smears out below T^*. Such a phenomenon can not be connected to the magnetic effects because the corresponding linewidth does not exhibit a dramatic broadening across the phase transition. Hence the NMR observation provides concrete evidence for the nonmagnetic origin for this phase transition. Since the NMR spectrum does appear as the Gaussian or Lorentzian forms, it is rather difficult to describe the degree of the line broadening by means of the linewidth versus temperature. Instead, we used the values of the broadening factor employed for the spectrum simulation as described below. The ratio of the broadening factors for 77 and 297 K is about 7.8 for the ^{59}Co NMR simulated spectra of $La_3Co_4Sn_{13}$, indicative of a moderate line broadening. The observed line broadening is mostly related to the inhomogeneity of the local electric field gradient (EFG) that is known to broaden the NMR transition lines. The spatial modulation of EFG due to incommensurate superlattices is a possible mechanism for the low-temperature line broadening in $La_3Co_4Sn_{13}$.

TABLE I. Quadrupole frequency in megahertz, anisotropic and isotropic Knight shifts in percent, experimental $1/T_1T$ in $s^{-1}K^{-1}$, and deduced partial Co 3*d* Fermi level DOS in units of states/eV f.u. for La_3Co_4 Sn_{13} above and below T^*.

Parameter	ν_Q	K_{an}	K_{iso}	$1/T_1T$	$N_d(E_F)$
$T > T^*$	1.42	−0.136	0.203	0.797	5.2
$T < T^*$	1.29	−0.126	0.193	0.688	4.8

The quadrupole frequency ν_Q can be determined directly from the satellite lines because the first order quadrupole shift is the major effect shaping these lines. On this basis, we obtained $\nu_Q = 1.42 \pm 0.02$ MHz for 297 K and $\nu_Q = 1.29 \pm 0.02$ MHz for 77 K, respectively. Both values were tabulated in Table I. Here, $\nu_Q = 3eQV_{zz}/[2I(2I-1)h]$ is defined by the nuclear quadrupole moment Q and the largest principal axis component of the EFG tensor V_{zz}. Hence the decrease in ν_Q below T^* suggests that the local EFG becomes weaker across the phase transition. The EFG sensed by the Co site of $La_3Co_4Sn_{13}$ may arise from the noncubic arrangement of the charged lattice ions and/or the nonuniform charge density of the conduction electrons. Attempts to reproduce the observed EFG with a simple point-charge model yield unreasonable charge transfers. With this respect, the redistribution of the inner core electrons would play a major role for the change in EFG. Therefore the reduced EFG could be accounted for by the decrease in the Co 3*d* electrons at low temperatures, being consistent with the result revealed by the spin-lattice relaxation rates.

For the combination of electric quadrupole and anisotropic Knight shift interactions, the shift of the transition lines can be expressed in the first order by[26]

$$\frac{\nu(m \to m-1)}{\nu_0} = 1 + \left[\frac{K_{an}}{2(1+K_{iso})} + \frac{\nu_Q}{2\nu_o}\left(m - \frac{1}{2}\right)\right] \times (3\cos^2\theta - 1). \quad (1)$$

Here, ν_o is the frequency at the centroid of the resonance, K_{iso} is the isotropic Knight shift, K_{an} is the anisotropic Knight shift, and θ is the angle between the crystal symmetry axis and the external magnetic field. The line-shape function was simulated, following Cohen and Reif,[27]

$$P(\nu - \nu_o) = \frac{1}{2}\left|\frac{d\nu}{d\cos\theta}\right|^{-1}. \quad (2)$$

By substituting the determined ν_Q and tuning K_{an}, each synthetic profile can be reproduced with convolution where the Gaussian function was introduced. The width of the Gaussian function, which varies with temperature corresponds to a broadening factor, responsible for the NMR line broadening. For each temperature, the best-simulated result with a proper broadening factor was plotted as a dashed. The employed broadening factors are 0.0045 and 0.035 for 297 and 77 K, respectively. The simulations yielded the corresponding $K_{iso} = 0.203\%$ and $K_{an} = -0.136\%$ for 297 K and $K_{iso} = 0.193\%$ and $K_{an} = -0.126\%$ for 77 K. These parameters were also listed in Table I. Since the spin dipolar interaction between nuclear and electronic spins is the main effect for K_{an},[28,29] the

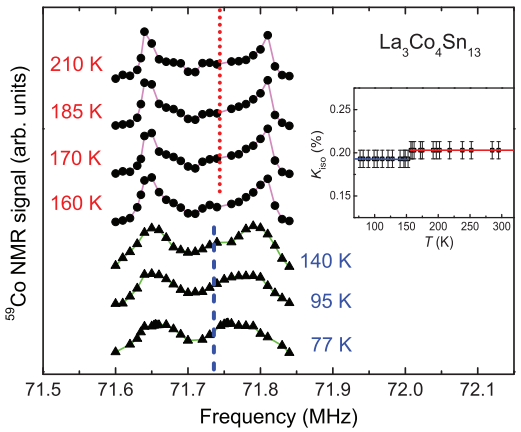

FIG. 5. (Color online) Evolution of ^{59}Co NMR central transition spectra of $La_3Co_4Sn_{13}$ measured below and above T^*. The dashed and dotted lines indicate the positions of the frequency at the centroid of the resonance below and above T^*, respectively. (Inset) Temperature dependence of the ^{59}Co NMR K_{iso} for $La_3Co_4Sn_{13}$.

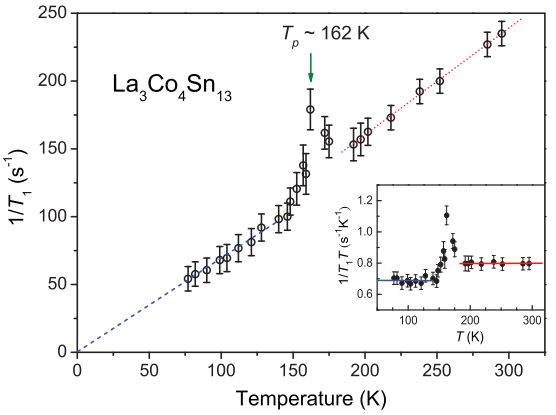

FIG. 6. (Color online) Temperature variation of the ^{59}Co spin-lattice relaxation rate for $La_3Co_4Sn_{13}$. A well-defined peak at $T_p \simeq 162$ K was indicated by an arrow. Two straight lines below and above T^* indicate the change in the slope of $1/T_1$ across the phase transition. (Inset) Plot of $1/T_1T$ vs T with two horizontal lines demonstrating the reduction in the magnitude of $1/T_1T$ below T^*.

slight decrease in the magnitude of K_{an} below T^* suggests a marginal change for this interaction.

To gain more insight into the evolution of the isotropic Knight shift across the transition, several representative central transition ($m = \frac{1}{2} \leftrightarrow -\frac{1}{2}$) spectra taken below and above T^* are displayed in Fig. 5. The corresponding temperature-dependent K_{iso} of $La_3Co_4Sn_{13}$ is shown in the inset of Fig. 5, indicating little or no change in K_{iso} across the phase transition. For the present case of $La_3Co_4Sn_{13}$, K_{iso} is the combination of the effects of the s contact, core polarization arising from d electrons, as well as the orbital shift. Because of the different sign and magnitude of the hyperfine fields from Co s and d electrons, it is rather difficult to separate these origins unambiguously from the Knight-shift analysis. It is worthwhile mentioning that the shape of the central resonance line is quite complex owing to the simultaneous presence of the anisotropic Knight shift and second-order quadrupole effects. Here, the variation in ν_Q below T^* has a minor effect on the distortion of the central resonance spectrum but the effect of K_{an} is a key origin responsible for the central line-shape change. It is apparent that the central resonance line in the previous case of $Ce_3Co_4Sn_{13}$ deforms more dramatically as compared to that in $La_3Co_4Sn_{13}$.[11] We found that K_{an} changes from -0.09% to -0.052% across the transition temperature in $Ce_3Co_4Sn_{13}$, while a marginal decrease of K_{an} (from -0.136% to -0.126%) was obtained in $La_3Co_4Sn_{13}$. This comparison clearly indicates that a substantial change in K_{an} for $Ce_3Co_4Sn_{13}$ is essentially responsible for the serious line shape deformation as observed.

While associating the Knight shift with specific electronic changes is complicated by a mixture of quadrupole and orbital shifts, the spin-lattice relaxation rate ($1/T_1$) is comparatively simple as it is mainly dominated by the conduction electrons. It thus provides a direct and quantitative probe of Fermi surface features for this system. The spin-lattice-relaxation time measurements were carried out using the inversion recovery method. We found each T_1 by centering the transmission frequency at the central transition resonance line and recorded the signal strength by integrating the recovered spin echo signal. For the central transition with $I = \frac{7}{2}$, the relaxation process of the nuclear magnetization involves the adjacent pairs of spin levels, and the corresponding recovery of the nuclear magnetization obeys[30]

$$\frac{M(t) - M(\infty)}{M(\infty)} = -2\alpha\left(0.012e^{-\frac{t}{T_1}} + 0.068e^{-\frac{6t}{T_1}} + 0.206e^{-\frac{15t}{T_1}} + 0.714e^{-\frac{28t}{T_1}}\right). \quad (3)$$

Here, $M(t)$ is the nuclear magnetization at the recovery time t and $M(\infty)$ is the magnetization after long-time recovery. The parameter α is a fractional value derived from the initial conditions used in our experiments. Each experimental T_1 was thus obtained by fitting to this multiexponential recovery curve.

The main panel of Fig. 6 illustrates the temperature variation of $1/T_1$ for $La_3Co_4Sn_{13}$ with a clear peak at around $T_p \simeq 162$ K. This temperature is higher than T^* determined from the specific heat measurement. Such a discrepancy suggestscomplicated mechanisms for the enhancement of the relaxation rates. Since a magnetic origin of the phase transition has been ruled out, the observed peak can not be interpreted as a result of the rapid fluctuations of the spin dynamics arising from magnetic ordering. We believe that the increase in $1/T_1$ can not be accounted for by critical fluctuations at the critical temperature which usually peaks at the critical temperature. Qualitatively, the contribution to $1/T_1$ due to thermally driven normal modes of the CDW is a likely source for the increase in the ^{59}Co NMR relaxation rate of $La_3Co_4Sn_{13}$,[31] and the peak feature is quite similar to that observed in the typical CDW ordering of $NbSe_3$.[32]

In spite of the peak, it is found that $1/T_1$ obeys the Korringa relation (constant T_1T) below and above T^*, and the result of $1/T_1T$ as a function of temperature is shown in the inset of Fig. 6. From the magnitude of $1/T_1T$, we could estimate the Co $3d$ partial Fermi level DOS below and above the phase transition of $La_3Co_4Sn_{13}$. For the d-spin

relaxation in metals, two relaxation mechanisms dominate the Korringa relation: $1/T_1T = (1/T_1T)_d + (1/T_1T)_{\rm orb}$. The first term arises from the d-spin core polarization, while the second one is due to the orbital electrons. Based on the non-interacting electron scenario, $(1/T_1T)_d$ and $(1/T_1T)_{\rm orb}$ can be expressed as[33]

$$\left(\frac{1}{T_1T}\right)_d = 2hk_B\left[\gamma_n H_{\rm hf}^d N_d(E_F)\right]^2\left[\frac{1}{3}f^2 + \frac{1}{2}(1-f)^2\right]q, \tag{4}$$

$$\left(\frac{1}{T_1T}\right)_{\rm orb} = 2hk_B\left[\gamma_n H_{\rm hf}^{\rm orb} N_d(E_F)\right]^2\left[\frac{2}{3}f\left(2-\frac{5}{3}f\right)\right]q, \tag{5}$$

where h and k_B are the Planck constant and the Boltzmann constant, respectively. γ_n is the Co nuclear gyromagnetic ratio and $N_d(E_F)$ is the partial Co $3d$ DOS at E_F in units of states/eV spin. $H_{\rm hf}^d$ and $H_{\rm hf}^{\rm orb}$ represent the hyperfine field per spin of the Co d electrons and the orbital hyperfine field per unit orbital angular momentum, respectively. The parameter f is the relative weight of the d orbitals in the t_{2g} states around E_F,[34] and q is a factor equal to the reciprocal of the degeneracy.

As revealed from the band structure calculation on $La_3Co_4Sn_{13}$,[18] the ratio of the Co $3d$ orbitals in the t_{2g} and e_g states is approximately 7 : 3 at E_F, yielding the magnitude of $f \sim 0.7$. Furthermore, there are two energy bands crossing the Fermi energy of $La_3Co_4Sn_{13}$, giving $q = 1/2$. Taking $H_{\rm hf}^d \sim -1.8 \times 10^5$ G in Co metals and $H_{\rm hf}^{\rm orb} \sim 5.7 \times 10^5$ G,[34,35] each $N_d(E_F)$ can be extracted from the combination of Eqs. (4) and (5) with experimental values of $1/T_1T$. We thus obtained $N_d(E_F) = 5.2$ states/eV f.u. for $T > T^*$ and $N_d(E_F) = 4.8$ states/eV f.u. for $T < T^*$, respectively. These results clearly demonstrate that $N_d(E_F)$ in $La_3Co_4Sn_{13}$ is reduced by 7.7% across the phase transition. Such a reduction in the electronic DOS implies that only a small segment of the Fermi surfaces is gapped below T^*.

III. DISCUSSION

The present investigation shows clear evidence for a first-order phase transition at around 152 K in $La_3Co_4Sn_{13}$ involved with a significant changes in electronic structures. The change of the electronic states can be realized as the slight movement and/or distortion of the Sn(2) atom from its initial position because this site resides at the only crystallographic site showing an active spatial degree of freedom within the structure. Such an interpretation has been confirmed by the temperature-dependent XRD measurements on the isostructural compounds of $Sr_3Ir_4Sn_{13}$ and $Ce_3Co_4Sn_{13}$.[14,36] This would give rise to a possible nesting of Fermi surfaces, and thus facilitate the CDW formation. As a matter of fact, partially gapping of the Fermi surfaces with a factor of 7.7% reduction in $N_d(E_F)$ has been revealed from our NMR T_1 analysis.

There is general agreement that CDW transitions usually take place in compounds with low-dimensional characters in their crystallographic structures, due to the instability at low temperatures against a periodic lattice distortion.[37,38] The CDW behavior in materials with 3D crystal structures is not ubiquitous. Rare-earth transition-metal ternary silicides with 3D crystallographic structures, such as the $R_5T_4Si_{10}$ and $R_2T_3Si_5$ types, have been shown to exhibit CDW phase transitions with remarkable anomalies observable in the thermal and electrical transport measurements.[17,24,39–48] While the physical origin of the CDW formation in this class of materials is largely unknown due to a lack of detailed band structure calculations, it is believed that the intricate balance and competition of different electronic states could play a critical role and affect the details of the CDW phase transition. A transmission electron microscopy (TEM) study of CDW in $Ho_5Ir_4Si_{10}$ indicated that the CDW phase transition was accompanied by a concomitant cell-doubling crystallographic structural phase transition.[44] A recent report also strongly suggested that CDW in $Lu_2Ir_3Si_5$ was accompanied by a similar structural phase transition.[47] With these respects, it seems that the simultaneous presence of a structure distortion with double cell parameters in their low-temperature phases is an important ingredient for triggering the nesting geometry around the Fermi surface, leading to the CDW formation within 3D crystallographic structures.

As mentioned, $La_3Co_4Sn_{13}$ exhibits a structural change from a simple cubic to a body centered cubic superstructure with crystallographic cell-doubling below 150 K.[20] This phenomenon is in reminiscence of those found in $Ho_5Ir_4Si_{10}$ and $Lu_2Ir_3Si_5$, suggesting the possible appearance of the CDW with the Fermi surface nesting in this material. From the theoretical band structure calculation in $La_3Co_4Sn_{13}$,[18] the band Nos. 391 and 392 exhibit flat curvature regions which are strong candidates for the nesting of Fermi surfaces. Likewise, the calculated band structure in $Sr_3Ir_4Sn_{13}$ shows that the flat sections of the band No. 329 could be responsible for the Fermi surface reconstruction.[14]The contribution of this band to the real part of the wave vector dependent charge susceptibility $\chi(\mathbf{q})$ shows a peak at $\mathbf{q} = (1/2, 1/2, 1/2)$, responsible for the Fermi surface nesting along a body diagonal direction within its 3D crystallographic structure. In fact, a considerable reduction of about 30% in the total Fermi level DOS has been estimated from the magnetic susceptibility of $Sr_3Ir_4Sn_{13}$,[14] implying a nesting instability with the wave vector $\mathbf{q} = (1/2, 1/2, 1/2)$. Due to the crystallographic similarity, we speculate a possible modulation wave vector along the same direction of (1/2, 1/2, 1/2) in $La_3Co_4Sn_{13}$. Further analyses of x-ray superlattice reflections and/or TEM images below T^* would be needed to verify the nesting vector in $La_3Co_4Sn_{13}$.

IV. CONCLUSIONS

In conclusion, $La_3Co_4Sn_{13}$ undergoing a first-order phase transition near 152 K has been identified by the specific heat measurement. NMR results further provide a concise picture for the changes in the local electronic properties. Concrete evidence for the reduction in the Fermi level DOS across this phase transition has been established. The phase transition in $La_3Co_4Sn_{13}$ essentially associated with partially gapped Fermi surfaces is very likely related to the CDW instability accompanied by lattice distortions. Remarkably, many aspects derived from this study in $La_3Co_4Sn_{13}$ are in resemblance to those found in the isostructural analog of

$Sr_3Ir_4Sn_{13}$. Namely, a cell-doubling crystallographic structural phase transition coexisting with superconductivity has been observed in both $La_3Co_4Sn_{13}$ and $Sr_3Ir_4Sn_{13}$. It thus points to a uniformity in the interplay between the structural instability and superconductivity within the materials of the $R_3T_4Sn_{13}$ prototype.

ACKNOWLEDGMENTS

This work was supported by the National Science Council of Taiwan under Grant Nos. NSC-101-2112-M-006-009-MY2 (CSL) and NSC-100-2628-M-259-001-MY3 (YKK).

*cslue@mail.ncku.edu.tw

†ykkuo@mail.ndhu.edu.tw

[1] J. P. Remeika, G. P. Espinosa, A. S. Cooper, H. Barz, Z. Fisk, L. D. Woolf, H. C. Hamaker, M. B. Maple, G. Shirane, and W. Thomlinson, Solid State Commun. **34**, 923 (1980).

[2] H. Sato, T. Fukuhara, S. Iwakawa, Y. Aoki, I. Sakamoto, S. Takayanagi, and N. Wada, Physica B **186-188**, 630 (1993).

[3] A. Rojek, C. Sulkowski, and K. Rogacki, Physica C **223**, 111 (1994).

[4] C. V. Tomy, G. Balakrishnan, and D. M. Paul, Phys. Rev. B **56**, 8346 (1997).

[5] C. Israel, E. M. Bittar, O. E. Aguero, R. R. Urbano, C. Rettori, I. Torriani, P. G. Pagliuso, N. O. Moreno, J. D. Thompson, M. F. Hundley, J. L. Sarrao, and H. A. Borges, Physica B **359-361**, 251 (2005).

[6] E. L. Thomas, H. O. Lee, A. N. Bankston, S. MaQuilon, P. Klavins, M. Moldovan, D. P. Young, Z. Fisk, and J. Y. Chan, J. Solid State Chem. **179**, 1642 (2006).

[7] U. Kohler, A. P. Pikul, N. Oeschler, T. Westerkamp, A. M. Strydom, and F. Steglich, J. Phys.: Condens. Matter **19**, 386207 (2007).

[8] M. Gamza, W. Schnelle, A. Slebarski, U. Burkhardt, R. Gumeniuk, and H. Rosner, J. Phys.: Condens. Matter **20**, 395208 (2008).

[9] J. Yang, B. Chen, C. Michioka, and K. Yoshimura, J. Phys. Soc. Jpn. **79**, 113705 (2010).

[10] N. Kase, H. Hayamizu, and J. Akimitsu, Phys. Rev. B **83**, 184509 (2011).

[11] C. S. Lue, H. F. Liu, S. L. Hsu, M. W. Chu, H. Y. Liao, and Y. K. Kuo, Phys. Rev. B **85**, 205120 (2012).

[12] K. Wang and C. Petrovic, Phys. Rev. B **86**, 024522 (2012).

[13] S. Y. Zhou, H. Zhang, X. C. Hong, B. Y. Pan, X. Qiu, W. N. Dong, X. L. Li, and S. Y. Li, Phys. Rev. B **86**, 064504 (2012).

[14] L. E. Klintberg, S. K. Goh, P. L. Alireza, P. J. Saines, D. A. Tompsett, P. W. Logg, J. Yang, B. Chen, K. Yoshimura, and F. M. Grosche, Phys. Rev. Lett. **109**, 237008 (2012).

[15] S. K. Goh, L. E. Klintberg, P. L. Alireza, D. A. Tompsett, J. Yang, B. Chen, K. Yoshimura, and F. M. Grosche, arXiv:1105.3941.

[16] S. Gerber, J. L. Gavilano, M. Medarde, V. Pomjakushin, C. Baines, E. Pomjakushina, K. Conder, and M. Kenzelmann, Phys. Rev. B. **88**, 104505 (2013).

[17] R. N. Shelton, L. S. Hausermann-Berg, P. Klavins, H. D. Yang, M. S. Anderson, and C. A. Swenson, Phys. Rev. B **34**, 4590 (1986).

[18] G. Zhong, X. Lei, and J. Mao, Phys. Rev. B **79**, 094424 (2009).

[19] N. Kase, H. Hayamizu, K. Inoue, and J. Akimitsu, Physica C **471**, 711 (2011).

[20] O. E. Aguero, Ph.D. thesis, University of Campinas, Brazil, 2006.

[21] C. S. Lue, S. H. Yang, A. Abhyankar, Y. D. Hsu, H. T. Hong, and Y. K. Kuo, Phys. Rev. B **82**, 045111 (2010).

[22] C. S. Lue, C. F. Chen, Fu-Kuo Chiang, and M.-W. Chu, Phys. Rev. B **80**, 174202 (2009).

[23] J. L. Hodeau, J. Chenavas, M. Marezio, and J. P. Remeika, Solid State Commun. **36**, 839 (1980).

[24] Y.-K. Kuo, C. S. Lue, F. H. Hsu, H. H. Li, and H. D. Yang, Phys. Rev. B **64**, 125124 (2001).

[25] C. S. Lue and S. C. Chen, Phys. Rev. B **79**, 125108 (2009).

[26] W. H. Jones, Jr., T. P. Graham, and R. G. Barnes, Phys. Rev. **132**, 1898 (1963).

[27] M. H. Cohen and F. Reif, in *Solid State Physics*, edited by F. Seitz and D. Turnbull (Academic, New York, 1957), Vol. 5, p. 311.

[28] A. Rubens, B. deCastro, and R. T. Schumacher, Phys. Rev. B **7**, 105 (1973).

[29] G. S. Tripathi, L. K. Das, P. K. Misra, and S. D. Mahanti, Phys. Rev. B **25**, 3091 (1982).

[30] A. Narath, Phys. Rev. **162**, 320 (1967).

[31] R. Blinc, Phys. Rep. **79**, 331 (1981).

[32] B. H. Suits and C. P. Slichter, Phys. Rev. B **29**, 41 (1984).

[33] B. Nowak, Solid State Nucl. Magn. Reson. **21**, 53 (2002).

[34] G. N. Rao, Hyperfine Interact. **7**, 141 (1979).

[35] C. S. Lue, Y. T. Lin, and C. N. Kuo, Phys. Rev. B **75**, 075113 (2007).

[36] A. Sebarski, B. D. White, M. Fijalkowski, J. Goraus, J. J. Hamlin, and M. B. Maple, Phys. Rev. B **86**, 205113 (2012).

[37] H. Frohlich, Proc. R. Soc. London A **223**, 296 (1954).

[38] R. E. Peierls, *Quantum Theory of Solids* (Oxford University Press, London, 1955), p. 108.

[39] B. Becker, N. G. Patil, S. Ramakrishnan, A. A. Menovsky, G. J. Nieuwenhuys, J. A. Mydosh, M. Kohgi, and K. Iwasa, Phys. Rev. B **59**, 7266 (1999).

[40] Y. K. Kuo, F. H. Hsu, H. H. Li, H. L. Huang, C. W. Huang, C. S. Lue, and H. D. Yang, Phys. Rev. B **67**, 195101 (2003).

[41] S. Van Smaalen, Acta Crystallogr. A **61**, 51 (2005).

[42] Y. Singh, D. Pal, S. Ramakrishnan, A. M. Awasthi, and S. K. Malik, Phys. Rev. B **71**, 045109 (2005).

[43] Y. K. Kuo, K. M. Sivakumar, T. H. Su, and C. S. Lue, Phys. Rev. B **74**, 045115 (2006).

[44] C. M. Tseng, C. H. Chen, and H. D. Yang, Phys. Rev. B **77**, 155131 (2008).

[45] R. Tediosi, F. Carbone, A. B. Kuzmenko, J. Teyssier, D. van der Marel, and J. A. Mydosh, Phys. Rev. B **80**, 035107 (2009).

[46] F. Galli, S. Ramakrishnan, T. Taniguchi, G. J. Nieuwenhuys, J. A. Mydosh, S. Geupel, J. Ludecke, and S. van Smaalen, Phys. Rev. Lett. **85**, 158 (2000).

[47] M. H. Lee, C. H. Chen, M.-W. Chu, C. S. Lue, and Y. K. Kuo, Phys. Rev. B **83**, 155121 (2011).

[48] N. S. Sangeetha, A. Thamizhavel, C. V. Tomy, S. Basu, A. M. Awasthi, S. Ramakrishnan, and D. Pal, Phys. Rev. B **86**, 024524 (2012).